IEEE Access
Multidisciplinary | Rapid Review | Open Access Journal

Received March 3, 2020, accepted March 24, 2020, date of publication March 30, 2020, date of current version April 16, 2020.

Digital Object Identifier 10.1109/ACCESS.2020.2984353

Three-Dimensional Geometric Descent Guidance With Impact Angle Constraint

HAO ZHOU, TAO CHENG, XIAOMING LIU, AND WANCHUN CHEN
School of Astronautics, Beihang university, Beijing 100191, China
Corresponding author : Xiaoming Liu (liuxiaoming_bh@163.com)

ABSTRACT A novel trajectory-shaping guidance law with impact angle constraint is proposed for attacking stationary targets in a three-dimensional environment. The guidance concept, derived from the inverse dynamic method, is to design an analytical curve trajectory satisfying the impact angle in advance and obtain reasonable control commands. The vehicle motion is decomposed in the horizontal and vertical planes of the inertial coordinate system. Firstly, the trajectory in the vertical plane is designed as ellipse, which can be shaped by adjusting its axis direction. An improved sliding mode control (SMC) method, which adds position-dependent correction to the weight in sliding mode surface, is adopted to track the nominal trajectory. Therefore, the vehicle approaches the ellipse quickly and smoothly in the early stage and hits the stationary target accurately. Secondly, a third-order Bézier curve with adjustable parameters is employed as the prior nominal trajectory in the lateral plane. When the vehicle deviates from the original trajectory due to perturbation or self-limitation, it will turn to the updated curve in real time according to its own condition. Moreover, coupling of acceleration commands in the two planes is resolved through acceleration decomposition, which qualifies independent trajectory design in two planes and paves a new way to more curve combinations. Nominal testing and Monte Carlo simulations on the proposed method are carried out. Simulation results demonstrate that the proposed guidance law is highly designable and strongly robust.

INDEX TERMS Hypersonic vehicle, geometric guidance, elliptic guidance, descent guidance.

I. INTRODUCTION

In terminal guidance, the basic goal for a missile or vehicle is to achieve a near-zero miss distance. Since the impact angle has large ramifications on kill performance, maneuvering ability, cooperative strike, etc., a specific impact angle is usually required in advanced guidance law designs.

Plenty of techniques have been suggested for the design of guidance algorithms, and proportional navigation guidance (PNG) is a classical guidance law. True PNG, which means the acceleration command is perpendicular to the line of sight (LOS), is variously ameliorated to achieve specific impact angle or flight time. A common refinement is to add a bias term to PNG, so that the impact angle can be attained under the premise of zero miss distance. Such bias is diverse and can be selected according to constraints. In [1], Kim proposed the bias proportional navigation guidance (BPNG) to realize desired impact angle and verified its optimality. In [2], Erer and Merttopçuoĝlu deduced the intercept angle increment caused by the bias, and divided a trajectory into two stages. When the terminal angle caused by integrated bias is equal to the desired angle, an unbiased PNG is adopted instead. In [3], an exponential bias is applied when the field-of-view (FOV) and acceleration constraints are employed. However, these two-stage BPNG methods are prone to generate abrupt acceleration commands. Park [4] deduced the terminal impact angle of PNG, and essentially constructed the state feedback contributing to smoother acceleration commands. Another refinement is to choose appropriate proportional gains, which can be piecewise or time-varying. In [5], Ratnoo and Ghose designed an orientation trajectory for initial phase with navigation gain $N < 2$. Although the acceleration risks being discontinuous, the missile can switch to $N \geq 2$ to achieve any desired impact angle averting singularity phenomenon. Considering the FOV and acceleration constraints, more methods for selecting gains are listed in [6], [7]. In [8], Liu *et al.* combined the optimal control and the PNG method, and solved this optimal control problem by numerical method. As a result, an off-line closed-loop gain optimization strategy was proposed. Although PNG and its modifications are simple in form, most of these methods inevitably rely on the measurement of LOS angle and its rate.

The associate editor coordinating the review of this manuscript and approving it for publication was Xiwang Dong.

Optimal guidance (OG) laws have attracted extensive interest due to minimum energy and multiple constraints. Assuming small deviations from a collision triangle, most of OG are developed by solving linearizing equations near the LOS. Kim and Grider [9] seems to be the first to propose the linear quadratic optimal guidance (LQOG) problem, and applied Riccati equation to solve the feedback gain for constrained angle requirement. In [10], Ryoo *et al.* proposed the optimal impact angle guidance law for lag-free and first-order autopilot. By using the third-order polynomial of range-to-go to express the optimal trajectory, a more accurate estimation of time-to-go is given to improve the accuracy of OG. In [11], Shaferman and Shima proposed the LQOG with known target maneuver and further developed a linear quadratic differential game guidance law assuming optimal target maneuver. However, the linear equation under the assumption of small deviation is not always applicable to the actual engagement scenario, so various simple restrictions are employed. In [12], [13], the nonlinear feedback for quasilinear equation is obtained by solving the state-dependent Riccati equation (SDRE), and any impact angle can be achieved in specific rotated frame. In [14], Taub and Shima proposed fast feedback solutions under time-varying acceleration bounds. In [15], [16], Park *et al.* considered the FOV constraint, and divided the trajectory into three segments according to whether the equation constraint are satisfied. Unlike the piecewise navigation gain for PNG, acceleration command in each segment is solved by the optimal control. In [17], the optimal trajectory with the impact angle requirement can be refined to achieve desired time by compensating for the time-to-go prediction error. In general, the optimal control method can ensure the optimal maneuvering under different conditions and analytical solutions for linear system are beneficial for on-line planning. Nevertheless, the optimization often requires high accuracy in modeling and measurement or estimation of various states, which makes it difficult to implement the guidance law.

As mentioned above, to deal with complex engagement modeling problem, nonlinear control can also be applied to devise guidance law. The common goal is to enforce both terminal LOS angle and its derivative to zero. The classical SMC method, which does not strictly necessitate a linear differential equation, can generate effective feedback control. In [18], Kumar *et al.* proposed nonsingular terminal sliding mode control (TSMC) that averts the terminal singular phenomenon. In [19], SMC method with FOV constraints is presented, which avoids the abrupt acceleration command like two-stage BPNG. In [20], sliding mode surfaces are constructed for both impact angle and time, and the stability conditions are obtained applying Lyapunov candidate functions. Besides, the superiority of SMC is that it can track the unsuspected acceleration of the target in terms of disturbance. In [21], Xiong *et al.* estimated the acceleration of the target with a linear extended state observer in TSMC, and performed excellent with respect to constant and sinusoidal maneuver. Zhang *et al.* [22] similarly exploited nonlinear disturbance observer in integral sliding mode control. In [23], Ji *et al.* used adaptive sliding mode control to estimate disturbance, and developed a continuous finite-time convergent robust guidance law in a three-dimensional environment. Other methods like feedback linearization in [24] and nonlinear mapping in [25] can also be employed for nonlinear control to realize the desired impact angle. Although the nonlinear control method cannot obtain an optimal solution, it is a more suitable trajectory planning method. Most importantly, high precision may be guaranteed when the target information is unknown.

The emerging guidance idea is prior design, which can devise the guidance law satisfying partial constraints in advance. Especially in guidance laws considering impact time, this idea is often applied by constructing the control related to the time-to-go. Therefore, a common prior design is to design acceleration command in advance. In [26], Kim *et al.* designed the acceleration as the time-to-go polynomial, which is optimal for lag-free system when the parameters are selected properly. In [27], three variables are used to construct augmented polynomials feedback satisfying the constraints of miss distance, impact angle and impact time simultaneously. Another prior design in trajectory-shaping is the inverse dynamic method, that is, to design trajectory in advance and deduce the control commands in reverse. Yakimenko [28], Yakimenko and Lukacs [29] designed the nominal trajectory in polynomial form and transformed it into a nonlinear optimization problem by inverse dynamics and obtained the suboptimal solution. Naghash *et al.* [30] designed Bézier curve trajectory under the constraint of acceleration and optimized parameters to maximize the terminal velocity. In [31], [32], Zhou applied neural network and secant method respectively to determine Bézier curve parameters satisfying impact angle and terminal velocity constraints. In [33], a circular trajectory could be updated by controlling LOS angle equal to the approach-angle error. Yoon [34] further proposed a relative circle guidance method for tracking moving target.

Most of the traditional guidance laws may be summarized as two-point guidance laws, which means the information between vehicle and target is required. In consequence, the implementation of guidance law depends on the measurement or estimation of complex parameters, such as time-to-go, LOS angle and its rate. In [35], Tsalik and Shima proposed the concept of three-point guidance, that is, launcher, missile and target are on the circular trajectory satisfying the impact angle constraint. In [36], this method is extended to attack moving target. Although the circular trajectory is generated in real time, the circle satisfying the constraints is unique. In [37], a nominal elliptical trajectory and the normal acceleration along it in the rotated frame are proposed, but the rotation angle is specific corresponding to flight path angle. In [38], Livermore developed the elliptic guidance law into a three-point guidance concept and applied a proportional–integral–derivative (PID) controller to track the ellipse. In conclusion, the three-point guidance concept is simple to implement and

suitable for trajectory planning. In essence, the concept of three-point guidance also utilizes the idea of inverse dynamics, except that control methods may be employed to track nominal trajectory. For the sake of simplicity, we refer to these methods of designing trajectories adopting properties of geometric curves as geometric guidance.

In this paper, a novel geometric guidance method in three-dimensional scenario is proposed for bank-to-turn hypersonic vehicle. The difficulty lies in the fact that when the vertical or lateral acceleration changes signs, the bank angle needs to be reversed quickly. However, the existence of constraints imposed on bank angle and its derivative limits lateral maneuver, so it is vital to adapt to the reversal bank angle requirement. As a result, a smooth geometric trajectory is designed in advance to achieve desired impact angle. The motion in vertical plane is to track elliptical trajectory, which is partly derived from [38], but the judgment method of ellipse existence is exactly given. To avoid undesired acceleration commands which frequently change signs, an improved SMC method based on a position-dependent weight is developed. The trajectory in lateral plane is a real-time updated Bézier curve, which can accommodate reversed bank angle commands and converge to desired impact direction. Nominal testing and 500-run Monte Carlo simulations on the proposed method are carried out.

The rest of paper is structured as follows: Section II presents the problem formulation for hypersonic vehicle descent guidance; Section III gives the derivation of the geometric guidance law and the complete guidance process; Section IV provides the simulation results to demonstrate the performance of the proposed method; Section V gives the conclusion.

II. PROBLEM FORMULATION

A. DESCENT DYNAMICS

Descent of a hypersonic vehicle is generally short in terms of range covered. As such, guidance law is developed assuming a flat earth and point mass vehicle. The dynamic equation can be formulated as

$$\begin{aligned}
&\dot{x} = V\cos\gamma\cos\psi, \quad \dot{y} = V\sin\gamma, \ \dot{z} = -V\cos\gamma\sin\psi \\
&\dot{\gamma} = \frac{L\cos\sigma}{mV} - \frac{g\cos\gamma}{V}, \quad \dot{\psi} = -\frac{L\sin\sigma}{mV\cos\gamma} \\
&\dot{V} = -\frac{D}{m} - g\sin\gamma
\end{aligned} \tag{1}$$

where, V is the velocity, γ is the flight path angle, ψ is the heading angle which is measured clockwise from the x-axis, σ is bank angle, and x, y, z are the position coordinates of the vehicle. L and D are aerodynamic lift and drag forces, which can be represented as

$$L = \frac{1}{2}\rho V^2 C_L S_{ref}, \quad D = \frac{1}{2}\rho V^2 C_D S_{ref} \tag{2}$$

where, ρ is the local atmospheric density, S_{ref} is the reference area. The terms, C_L and C_D, are the lift and drag coefficients, which can be simplified as

$$C_L = f_L(M_a, \alpha), \quad C_D = f_D(M_a, \alpha) \tag{3}$$

where, M_a is Mach number, α is angle of attack. In this paper, the two functions f_L, f_D are analytic functions after fitting, so the inverse functions can be obtained.

B. DESCENT TRAJECTORY CONSTRAINTS

Remark: In this paper, L, M, T represent "launch point", missile (or vehicle) and stationary target respectively, where "launch point" can be a selected point in terminal guidance. Variables with subscripts "L" and "T" represent the desired state of the missile (or vehicle) at the launch point and the target point, rather than the movement of the two fixed points. Except for normal overload $n_\perp$, all variables with "$\perp$" in the subscript represent projections in xy plane, while those with "H" are projections in xz plane (i.e., the horizontal plane). All variables in the rotated reference frame are denoted with prime superscript. Variables with "new" in the subscript are updated to simulate new Bézier curve.

Initial and terminal state constraints are formulated as

$$\begin{aligned}
&x(t_0) = x_L, \quad y(t_0) = y_L, \ z(t_0) = z_L \\
&V(t_0) = V_L, \quad \gamma(t_0) = \gamma_L, \ \psi(t_0) = \psi_L
\end{aligned} \tag{4}$$

$$\begin{aligned}
&x(t_f) = x_T, \quad y(t_f) = y_T, \ z(t_f) = z_T \\
&\gamma(t_f) = \gamma_T, \quad \psi(t_f) = \psi_T
\end{aligned} \tag{5}$$

The constraints imposed on the control and control derivatives are expressed as

$$\begin{aligned}
&\alpha_{\min} \le \alpha \le \alpha_{\max}, \quad |\dot{\alpha}| \le \dot{\alpha}_{\max} \\
&\sigma_{\min} \le \sigma \le \sigma_{\max}, \quad |\dot{\sigma}| \le \dot{\sigma}_{\max}
\end{aligned} \tag{6}$$

where α is the angle of attack, the terms, $\alpha_{\min}$, $\alpha_{\max}$, $\sigma_{\min}$, $\sigma_{\max}$, $\dot{\alpha}_{\min}$ and $\dot{\alpha}_{\max}$ are all given constant values.

The constraint imposed on normal load is shown in (7).

$$|n_\perp| \le n_{\perp\max} \tag{7}$$

III. GEOMETRIC GUIDANCE LAW

In this section, the vehicle motion is decomposed in the horizontal plane (xz plane) and the vertical plane (xy plane), and the nominal trajectory in each plane is designed independently. It is worth noting that the vertical plane is fixed with the coordinate system, rather than the plane including velocity vector. The nominal trajectory in xy plane is an ellipse, and an SMC tracking strategy is adopted. This method can effectively achieve tiny miss distance and avoid frequent reversal bank angles. The trajectory in xz plane is a real-time updated third-order Bézier curve, which adapts well to control constraints and accepts more flexible maneuvers. Fig.1 shows the design method of three-dimensional geometric trajectory.

A. ELLIPTIC GUIDANCE LAW

1) ELLIPTICAL TRAJECTORY DESIGN

A qualified elliptical trajectory needs to pass through two stationary points, $L_\perp$, $T_\perp$, and the corresponding tangent direction should be consistent with vector $\boldsymbol{V}_{L\perp}$ and $\boldsymbol{V}_{T\perp}$. Assuming an elliptical trajectory exists, in general, Fig.2 shows the trajectory if the vehicle strikes the target clockwise.

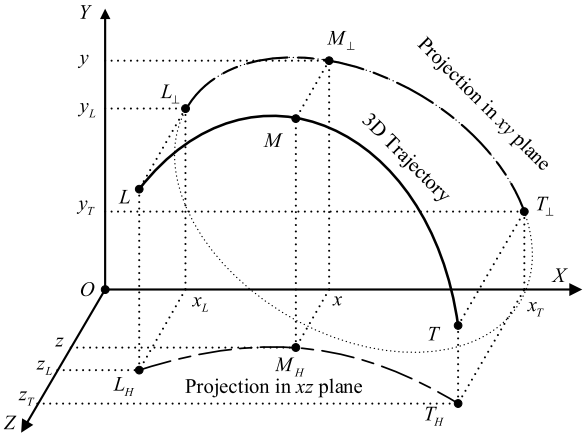

FIGURE 1. Three-dimensional geometric trajectory.

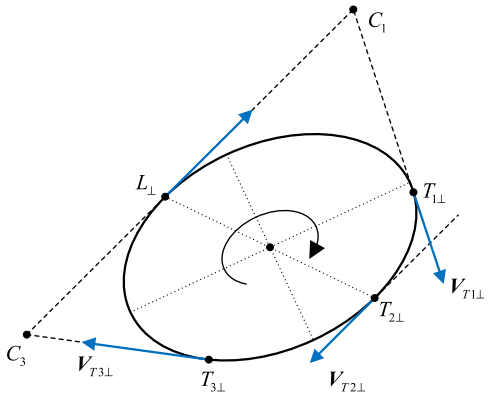

FIGURE 2. Elliptical trajectory in clockwise direction.

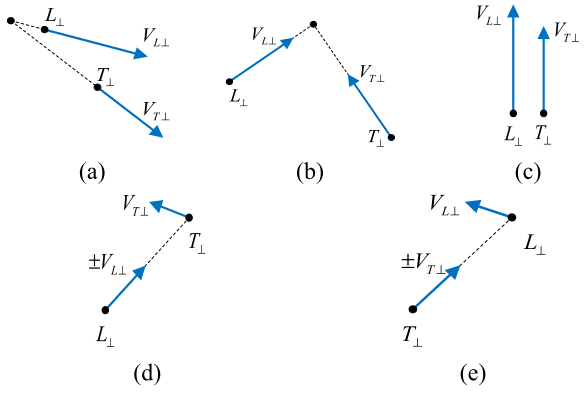

FIGURE 3. Several irrational design scenarios.

The distribution of three representative target points $T_{1\perp}$, $T_{2\perp}$ and $T_{3\perp}$ on the ellipse is given, and desired terminal velocity vectors are $\boldsymbol{V}_{T1\perp}$, $\boldsymbol{V}_{T2\perp}$ and $\boldsymbol{V}_{T3\perp}$. When there is an intersection between the desired launch velocity and terminal velocity (like C_1, C_3 in Fig.2), only one velocity vector points to the intersection. Otherwise, the terminal velocity is parallel and reverse to the launch direction (like $T_{2\perp}$ in Fig.2). Therefore, Fig.3 shows several classical scenarios where elliptical trajectory design will fail.

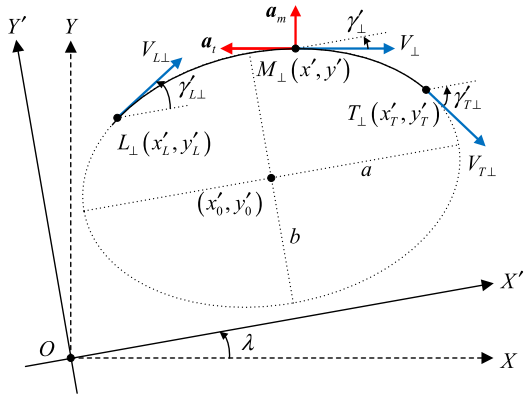

FIGURE 4. Nominal elliptical trajectory in rotated reference frame.

In this paper, an ellipse whose main axis is parallel to a certain axis of the reference frame is called a "standard ellipse". The "standard ellipse" equation is solved at a specific rotation angle in [37], [38], that is, the flight path angle at the launch point or the target point, without a general analytical expression. In fact, there is at most one "standard ellipse" after an arbitrary rotation angle is determined. The nominal elliptical trajectory in rotated reference frame is displayed in Fig.4.

In Fig.4, a_m is the normal acceleration required, a_t is the tangential acceleration, λ is the rotation angle of elliptical axis measured clockwise from the x-axis. The terms, a and b are the lengths of two semi-axis. The rotation coordinate relationship is represented as

$$\begin{cases} x'_i = x_i \cos(\lambda) + y_i \sin(\lambda) \\ y'_i = -x_i \sin(\lambda) + y_i \cos(\lambda) \\ \gamma'_{i\perp} = \gamma_{i\perp} - \lambda \end{cases}, i = L/T \tag{8}$$

The "standard ellipse" in the rotated reference frame is formulated as

$$\left(x' - x'_0\right)^2 \Big/ a^2 + \left(y' - y'_0\right)^2 \Big/ b^2 = 1 \tag{9}$$

The tangent slope at any point (x', y') on the ellipse can be expressed as:

$$\tan\gamma' = -b^2\left(x' - x'_0\right) \Big/ \left(a^2\left(y' - y'_0\right)\right) \tag{10}$$

When the parameter λ is determined, the elliptical trajectory parameters to be solved are a, b, x'_0 and y'_0. Assuming infinite tangent is allowed, the problem is to solve (11) and (12).

$$\begin{aligned} \left(x'_L - x'_0\right)^2 \Big/ a^2 + \left(y'_L - y'_0\right)^2 \Big/ b^2 &= 1 \\ \left(x'_T - x'_0\right)^2 \Big/ a^2 + \left(y'_T - y'_0\right)^2 \Big/ b^2 &= 1 \end{aligned} \tag{11}$$

$$\begin{aligned} \tan\gamma'_{L\perp} &= -b^2\left(x'_L - x'_0\right) \Big/ \left(a^2\left(y'_L - y'_0\right)\right) \\ \tan\gamma'_{T\perp} &= -b^2\left(x'_T - x'_0\right) \Big/ \left(a^2\left(y'_T - y'_0\right)\right) \end{aligned} \tag{12}$$

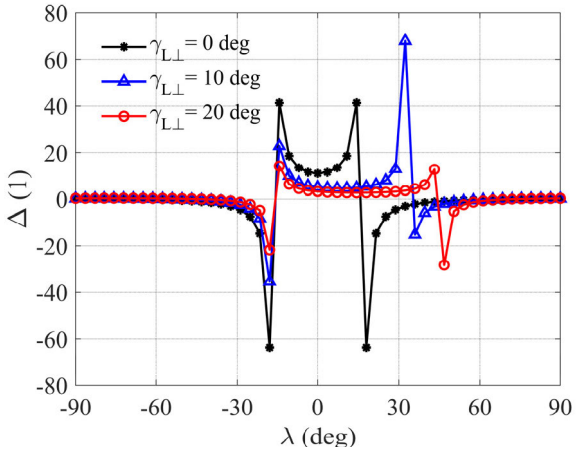

FIGURE 5. The change of judgment variable Δ with λ under different strike conditions.

To simplify the equation, the parametric equation is adopted as follows

$$\begin{cases} x'_L = a\sin\theta + x'_0, & y'_L = b\cos\theta + y'_0 \\ x'_T = a\sin\beta + x'_0, & y'_T = b\cos\beta + y'_0 \end{cases}, \theta, \beta \in [0, 2\pi) \tag{13}$$

Substituting (13) into (12) yields the following algebraic equation

$$-\left(b/a\right)\tan\theta = \tan\gamma'_{L\perp}, \quad -\left(b/a\right)\tan\beta = \tan\gamma'_{T\perp} \tag{14}$$

So far, the original problem is transformed into solving (13) and (14), and the parameters to be solved are a, b, θ, β, x'_0 and y'_0.In the case of $x'_L = x'_T$ or $y'_L = y'_T$, (13) leads to a simple conclusion, i.e., $\left|\tan\gamma'_L\right| = \left|\tan\gamma'_T\right|$, so that it is easy to judge whether a qualified elliptical trajectory exists. Therefore, the derivation in the following paper is based on $x'_L \neq x'_T$, $y'_L \neq y'_T$, and naturally $\left|\tan\gamma'_L\right| \neq \left|\tan\gamma'_T\right|$. After rearrangement, the simultaneous equation of (13) and (14) is formulated as

$$\frac{x'_L - x'_T}{y'_L - y'_T} = -\frac{a^2}{b^2}\frac{\tan\gamma'_{L\perp}/\cos\beta - \tan\gamma'_{T\perp}/\cos\theta}{1/\cos\beta - 1/\cos\theta} \tag{15}$$

In terms of (14), (15) can be converted into an equation about a/b, but the signs of $\cos\beta$ and $\cos\theta$ expect to be identified. However, after verifying each case, the signs do not affect the solution as (16), as shown at the bottom of this page, where λ_{LT} denotes the LOS angle between the launch point and the target in xy plane. Therefore, if and only if $\Delta > 0$, the ellipse exists and is unique. When $\Delta = 1$, the elliptical trajectory degenerates into a circle. Then, (14) can be simplified as

$$\tan\theta = -\sqrt{\Delta}\tan\gamma'_L, \quad \tan\beta = -\sqrt{\Delta}\tan\gamma'_T \tag{17}$$

Two simple inequality properties can be obtained by observing (13) and rearranging (17) as follows

$$\begin{cases} |\sin\theta| > |\sin\beta|, & if \ \left|\tan\gamma'_0\right| > \left|\tan\gamma'_f\right| \\ |\sin\theta| < |\sin\beta|, & if \ \left|\tan\gamma'_0\right| < \left|\tan\gamma'_f\right| \end{cases} \tag{18}$$

$$a = \left(x'_L - x'_T\right)/(\sin\theta - \sin\beta) > 0,$$
$$b = \left(y'_L - y'_T\right)/(\cos\theta - \cos\beta) > 0 \tag{19}$$

It can be concluded from (18) and (19) that the sign of a sine or cosine of θ and β can be determined as follows

$$\begin{cases} \left.\begin{array}{l} \sin\theta < 0, \ if \ x'_L < x'_T \\ \sin\theta > 0, \ if \ x'_L > x'_T \\ \cos\beta > 0, \ if \ y'_L < y'_T \\ \cos\beta < 0, \ if \ y'_L > y'_T \end{array}\right\} \ if \ \left|\tan\gamma'_0\right| > \left|\tan\gamma'_f\right| \\ \left.\begin{array}{l} \cos\theta < 0, \ if \ y'_L < y'_T \\ \cos\theta > 0, \ if \ y'_L > y'_T \\ \sin\beta > 0, \ if \ x'_L < x'_T \\ \sin\beta < 0, \ if \ x'_L > x'_T \end{array}\right\} \ if \ \left|\tan\gamma'_0\right| < \left|\tan\gamma'_f\right| \end{cases} \tag{20}$$

According to (17) and (20), the unique solution of θ and β in interval $[0, 2\pi)$ can be obtained. Then, all ellipse parameters can be solved by (13) and (19).

Fig.5 depicts the change of judgment variable Δ in (16) when $\gamma_{T\perp} = -90$ deg and the sampling interval is 0.02π. Apparently, it seems difficult to give an accurate range of λ from (16) with $\Delta > 0$, not to mention that there may not be an ellipse as shown in Fig.3. This phenomenon hinders the strategy of real-time updating ellipse, so that this paper adopts an effective tracking method. However, as shown in Fig.5, a continuous and effective interval of λ may be easy to obtain in some cases. Since Δ is only determined by four angles λ, λ_{LT}, $\gamma_{L\perp}$ and $\gamma_{T\perp}$, it is advisable to make an effective interval table of λ according to these angles.

To show the design effect of elliptical trajectory, a series of desired trajectories with launch point at (0 km,30 km) and target point at (100 km,0 km) are shown in Fig.6 and Fig.7. Fig.6 shows a series of trajectories with rotation angle $\lambda = 0$ deg, and various desired trajectory properties are shown in Table 1. It is apparent that the ellipse design adapts to various conditions even under a fixed rotation angle. Fig.7 shows the effect of λ on elliptical trajectories when $\gamma_{L\perp} = 20$ deg and $\gamma_{T\perp} = -90$ deg. Obviously, the only degree of freedom left, λ, shapes the elliptical trajectory substantially.

$$\begin{aligned} \Delta &= \Delta\left(\lambda, \lambda_{LT}, \gamma_{L\perp}, \gamma_{T\perp}\right) = a^2/b^2 \\ &= \frac{\sin\left(\gamma'_{L\perp} + \gamma'_{T\perp}\right) - 2\tan\left(\lambda'_{LT}\right)\cos\left(\gamma'_{L\perp}\right)\cos\left(\gamma'_{T\perp}\right)}{\tan^2\left(\lambda'_{LT}\right)\sin\left(\gamma'_{L\perp} + \gamma'_{T\perp}\right) - 2\tan\left(\lambda'_{LT}\right)\sin\left(\gamma'_{L\perp}\right)\sin\left(\gamma'_{T\perp}\right)} \end{aligned} \tag{16}$$

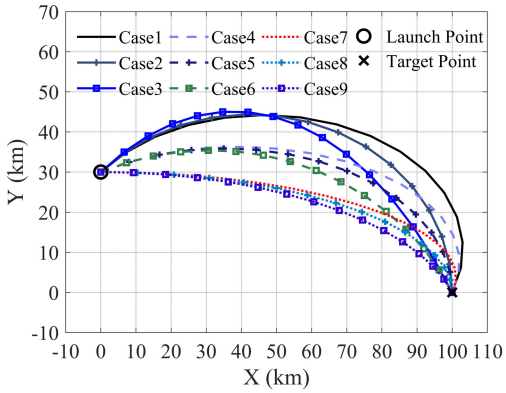

FIGURE 6. Elliptical trajectories when $\lambda = 0$ deg.

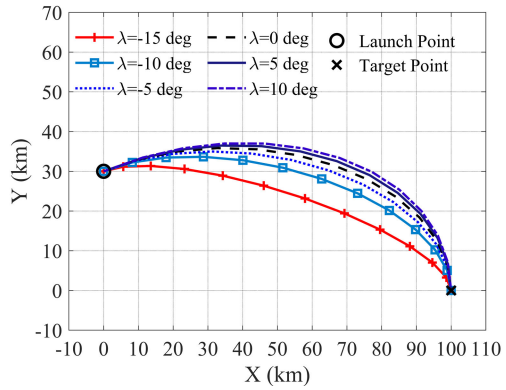

FIGURE 7. The effect of λ on elliptical trajectories.

TABLE 1. Desired trajectory properties for Fig. 6

Cases	$\gamma_{L\perp}$ (deg)	$\gamma_{T\perp}$ (deg)
Case 1	0	-110
Case 2	0	-90
Case 3	0	-70
Case 4	20	-110
Case 5	20	-90
Case 6	20	-70
Case 7	40	-100
Case 8	40	-90
Case 9	40	-70

In a nutshell, even though there is only one design parameter, the elliptical trajectory can be greatly adjusted.

2) IMPROVED SLIDING MODE GUIDANCE LAW

Inspired by [38], this paper guarantees the tracking effect by enforcing the sum of the distance between the vehicle and two foci constant. This simple guidance concept is the reason why the ellipse is chosen as a nominal trajectory. However, the PID control method does not adapt well to disturbance, because suitable general parameters may be difficult to obtain. Besides, PID tends to generate acceleration commands changing signs frequently, which leads to reverse bank angle requirement. Therefore, SMC is applied to ensure the stability of this nonlinear system.

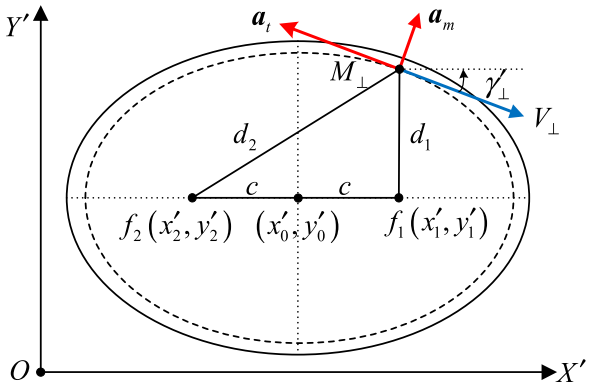

FIGURE 8. Elliptical trajectory tracking method.

The method for the vehicle to track the elliptical trajectory is displayed in Fig.8. The distances between the vehicle to foci f_1 and f_2 are marked as d_1 and d_2, respectively.

The foci $f_1\left(x_1', y_1'\right)$ and $f_2\left(x_2', y_2'\right)$ are defined in rotated reference frame as

$$\begin{cases} c = \sqrt{\left|a^2 - b^2\right|} \\ x_1' = x_0' + c, x_2' = x_0' - c, \quad y_1' = y_2' = y' \ (ifa \geq b) \\ y_1' = y_0' + c, y_2' = y_0' - c, \quad x_1' = x_2' = x_0' \ (ifa < b) \end{cases} \tag{21}$$

To apply SMC method, the desired signal $y_d(t)$ and tracking signal $y_t(t)$ are chosen as

$$\begin{aligned} y_d(t) &= 2\max\{a, b\} \\ y_t(t) &= d_1(t) + d_2(t) \end{aligned} \tag{22}$$

Any order derivative of the constant desired signal is zero, then of course, $\ddot{y}_d(t) = \dot{y}_d(t) = 0$. The common sliding surface and the corresponding reaching law are designed as

$$\begin{cases} S = (\dot{y}_t - \dot{y}_d) + \nu\,(y_t - y_d) \\ \dot{S} = -\varepsilon \mathrm{sat}(S/\phi) - KS \end{cases}, \varepsilon, \nu, K, \phi > 0 \tag{23}$$

where, ν, ε and K are weights. Saturation function $\mathrm{sat}(x)$ is defined as

$$\mathrm{sat}(x) = \begin{cases} x, & |x| \leq 1 \\ \mathrm{sgn}(x), & |x| > 1 \end{cases} \tag{24}$$

When ν approaches infinity, only the tracking error is considered, and the error on the sliding surface is zero. However, if ν is chosen too large, the trajectory will vibrate seriously in the early stage of terminal guidance, especially under the limited condition (6). If ν is too small, the tracking effect cannot be guaranteed. Therefore, (23) can be improved by steadily increasing the weight ν over time. Nominal trajectory determined in advance, the position can also be adopted to adjust the weight ν.

After added the power form weight correction term, the improved sliding surface is defined as

$$S = \dot{y}_t - \dot{y}_d + \left(\nu + \upsilon(x - x_0)^p / \left(x_f - x_0\right)^p\right)(y_t - y_d) \tag{25}$$

The derivative of sliding surface is expressed as

$$\dot{S} = \ddot{d}_1 + \ddot{d}_2 + \left(\nu + \upsilon(x - x_0)^p \big/ (x_f - x_0)^p\right)(\dot{y}_t - \dot{y}_d) + \upsilon p \dot{x}(y_t - y_d)(x - x_0)^{p-1} \big/ (x_f - x_0)^p \quad (26)$$

where

$$\begin{cases} d_i = \sqrt{(x' - x_i')^2 + (y' - y_i')^2} \\ \dot{d}_i = \left(\dot{x}'(x' - x_i') + \dot{y}'(y' - y_i')\right)/d_i \\ \ddot{d}_i = \left(V_\perp^2 - \dot{d}_i^2 + \ddot{x}'(x' - x_i') + \ddot{y}'(y' - y_i')\right)/d_i \end{cases}, i = 1, 2 \quad (27)$$

In terms of geometric properties, the first and second derivatives of x' and y' can be expressed as

$$\begin{aligned} \dot{x}' &= V_\perp \cos\gamma_\perp', \quad \ddot{x}' = -a_m \sin\gamma_\perp' - a_t \cos\gamma_\perp' \\ \dot{y}' &= V_\perp \sin\gamma_\perp', \quad \ddot{y}' = +a_m \cos\gamma_\perp' - a_t \sin\gamma_\perp' \end{aligned} \quad (28)$$

A notable property is that the tangential acceleration affects the velocity and the normal acceleration affects the trajectory shape. In fact, in case of small disturbance, the velocity vector approximately follows tangent direction of the dotted ellipse in Fig.8. If normal acceleration is appropriate, the vehicle moves approximately along the dotted ellipse, so the influence of a_t on $y_t(t)$ can be ignored.

Substituting (28) into (27) and ignoring the tangential acceleration leads to the following equation.

$$\begin{aligned} \ddot{y}_t(t) &= \ddot{d}_1 + \ddot{d}_2 \\ &\approx \left(V_\perp^2 - \dot{d}_1^2\right)\big/ d_1 + \left(V_\perp^2 - \dot{d}_2^2\right)\big/ d_2 \\ &\quad - \left((x' - x_1')/d_1 + (x' - x_2')/d_2\right)\sin\gamma_\perp' a_m \\ &\quad + \left((y' - y_1')/d_1 + (y' - y_2')/d_2\right)\cos\gamma_\perp' a_m \end{aligned} \quad (29)$$

When (29) is substituted, (26) can be simplified as

$$\dot{S} \approx b_{am} - k_{am} a_m \quad (30)$$

where, the terms b_{am}, c_{am} and k_{am} are defined as

$$\begin{aligned} b_{am} &= \left(V_\perp^2 - \dot{d}_1^2\right)\big/ d_1 + \left(V_\perp^2 - \dot{d}_2^2\right)\big/ d_2 \\ &\quad + \left(\nu + \upsilon(x - x_0)^p \big/ (x_f - x_0)^p\right)(\dot{d}_1 + \dot{d}_2) \\ &\quad + \upsilon p \dot{x}(y_t - y_d)(x - x_0)^{p-1} \big/ (x_f - x_0)^p \\ k_{am} &= \left((x' - x_1')/d_1 + (x' - x_2')/d_2\right)\sin\gamma_\perp' \\ &\quad - \left((y' - y_1')/d_1 + (y' - y_2')/d_2\right)\cos\gamma_\perp' \end{aligned} \quad (31)$$

To reduce the acceleration vibration, the approach velocity of the sliding surface is also weighted in the form of power. A novel reaching law is chosen as

$$\dot{S} = -\varepsilon sat(S/\phi)(x - x_0)^p \big/ (x_f - x_0)^p - KS \quad (32)$$

To prove its stability, Lyapunov function is chosen as

$$V_S = 0.5S^2 \geq 0 \quad (33)$$

The time derivative of V_S along (32) is

$$\begin{aligned} \dot{V}_S &= S\dot{S} \\ &= -\varepsilon(x - x_0)^p \big/ (x_f - x_0)^p S sat(S/\phi) - KS^2 \\ &= -\varepsilon(x - x_0)^p \big/ (x_f - x_0)^p \min\left(S^2/\phi, |S|\right) - KS^2 \\ &\leq 0 \end{aligned} \quad (34)$$

The reaching speed can be estimated as

$$\begin{cases} \dot{V}_S \leq -\varepsilon\left(\dfrac{x - x_0}{x_f - x_0}\right)^p \phi - K\phi^2, & if\ V_S \geq 0.5\phi^2 \\ \dot{V}_S = -2\left(\dfrac{\varepsilon}{\phi}\left(\dfrac{x - x_0}{x_f - x_0}\right)^p + K\right)V_S, & if\ V_S < 0.5\phi^2 \end{cases} \quad (35)$$

Obviously, the Lyapunov function will converge in finite time, and so will the sliding mode. Based on (32) and (35), (25) the significance and selection method of these six parameters can be concluded as

ν, υ, p: These three positive parameters are designed to adjust time constant of the first-order system in (25) when S = 0. The improved form allows large errors in the early stage and accurate terminal miss distance.

ε, K, p: Similarly, these parameters are applied to adjust the dynamic characteristics of system in (32).

ϕ: This parameter limits the reaching speed caused by excessive sliding mode, and thus improves the stability of the system.

Apparently, substitute (32) into (30) and rearrange it, normal acceleration can be expressed as

$$a_m = \frac{\varepsilon(x - x_0)^p \big/ (x_f - x_0)^p sat(S/\phi) + KS + b_{am}}{k_{am}} \quad (36)$$

where, positive parameters ε, ϕ, K, υ, ν and p are selected according to aerodynamic models and simulation conditions. Under small disturbance, the effect of normal acceleration on distance adjustment always exists, so there is no singular phenomenon, i.e., $k_{am} \neq 0$.

B. BÉZIER CURVE GUIDANCE LAW

In the early 1960s, Bézier curve was developed by Pierre Etienne Bézier and Paul de Faget de Casteljau. Bézier curve is defined as a spline function represented by polynomials on interval [0,1]. The trajectory shape can be adjusted by rearranging interpolation points, so it is widely employed in trajectory planning [28]–[32]. In [39], an standard definition of n-order Bézier curve is given as

$$P(\tau) = \sum_{i=0}^{n} B_i J_{n,i}(\tau), \quad \tau \in [0, 1] \quad (37)$$

where B_i are chosen weights and function $J_{n,i}(\tau)$ are defined as

$$J_{n,i}(\tau) = \frac{n!}{i!(n - i)!}\tau^i (1 - \tau)^{n-i} \quad (38)$$

The r-th derivative of Bézier curve is formulated as

$$d^r P(\tau)/d\tau^r = \left(n!/(n - r)!\right)\sum_{i=0}^{n-r} \Delta^r B_i J_{n-r,i}(\tau) \quad (39)$$

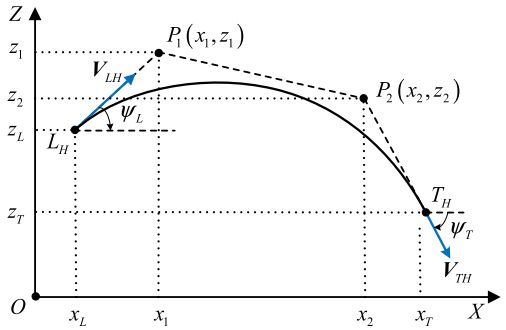

FIGURE 9. Third-order Bézier curve trajectory.

where

$$\begin{cases} \Delta^0 B_i = B_i \\ \Delta^k B_i = \Delta^{k-1} B_{i+1} - \Delta^{k-1} B_i \end{cases}, k = 1, 2 \cdots r \quad (40)$$

From (39) and (40), an sufficient and unnecessary condition for monotonicity of function P are formulated as follows

$$\begin{cases} \forall i, B_{i+1} - B_i > 0 \Rightarrow dP/d\tau > 0 \\ \forall i, B_{i+1} - B_i < 0 \Rightarrow dP/d\tau < 0 \end{cases}, i = 0, 1 \cdots n-1 \quad (41)$$

When the n-order Bézier curve is used to define an trajectory in xz plane, weights are selected as

$$B_{ix} = \begin{cases} x_L, & i = 0 \\ x_T, & i = n \\ x_i, & 0 < i < n \end{cases}, \quad B_{iz} = \begin{cases} z_L, & i = 0 \\ z_T, & i = n \\ z_i, & 0 < i < n \end{cases} \quad (42)$$

where B_{ix} and B_{iz} are weights for x and z coordinates, respectively. A third-order Bézier curve trajectory is depicted by Fig.9 in which ψ_L, $\psi_T \in (-0.5\pi, 0.5\pi)$.

To achieve the desired impact angle, the coordinates of the interpolation point are defined as follows

$$\begin{aligned} x_1 &= x_L + k_1 (x_T - x_L), \quad z_1 = z_L + \tan(-\psi_L)(x_1 - x_L) \\ x_2 &= x_L + k_2 (x_T - x_L), \quad z_2 = z_T - \tan(-\psi_T)(x_T - x_2) \end{aligned} \quad (43)$$

where k_1 and k_2 are adjustable parameters. From (37), (38) and (42), the curve is eventually formulated as:

$$\begin{cases} x = (1-\tau)^3 x_L + 3\tau(1-\tau)^2 x_1 + 3\tau^2(1-\tau) x_2 + \tau^3 x_T \\ z = (1-\tau)^3 z_L + 3\tau(1-\tau)^2 z_1 + 3\tau^2(1-\tau) z_2 + \tau^3 z_T \end{cases} \quad (44)$$

where $\tau = 0$ represents the starting point of the trajectory, and $\tau = 1$ represents the end. Without loss of generality, suppose $x_L < x_T$. To map x to τ, there should be $dx/d\tau > 0$. From (41), that is, $k_1 < k_2$. The first and second derivatives of the third-order Bézier curve with respect to τ are as follows

$$\begin{aligned} \frac{dx}{d\tau} &= -3\left((1-\tau)^2 x_L - \left(3\tau^2 - 4\tau + 1\right) x_1 \right. \\ &\quad \left. + \left(3\tau^2 - 2\tau\right) x_2 - \tau^2 x_T\right) \\ \frac{dz}{d\tau} &= -3\left((1-\tau)^2 z_L - \left(3\tau^2 - 4\tau + 1\right) z_1 \right. \\ &\quad \left. + \left(3\tau^2 - 2\tau\right) z_2 - \tau^2 z_T\right) \end{aligned} \quad (45)$$

$$\begin{aligned} \frac{d^2x}{d\tau^2} &= 6\left((1-\tau) x_L + (3\tau - 2) x_1 + (-3\tau + 1) x_2 + \tau x_T\right) \\ \frac{d^2z}{d\tau^2} &= 6\left((1-\tau) z_L + (3\tau - 2) z_1 + (-3\tau + 1) z_2 + \tau z_T\right) \end{aligned} \quad (46)$$

Radius of curvature ρ_n and lateral acceleration a_{zn} are defined as

$$\rho_n = \left(1 + \left(\frac{dz}{dx}\right)^2\right)^{1.5} \Big/ \frac{d^2z}{dx^2}, \quad a_{zn} = \frac{V_H^2}{\rho_n} \quad (47)$$

where

$$\frac{d^2z}{dx^2} = \frac{d\left(\frac{dz}{dx}\right)/d\tau}{dx/d\tau} = \left(\frac{d^2z}{d\tau^2} \cdot \frac{dx}{d\tau} - \frac{d^2x}{d\tau^2} \cdot \frac{dz}{d\tau}\right) \Big/ \left(\frac{dx}{d\tau}\right)^3 \quad (48)$$

The online updating strategy given in this paper is to ensure vehicle hits the target along the nominal trajectory when undisturbed. The preconditions for updating the trajectory are shown in (49) and (50).

$$\begin{aligned} x_{L,new} &\equiv x_L, \quad x_{T,new} \equiv x_T \\ x_{1,new} &\equiv x_1, \quad x_{2,new} \equiv x_2 \\ z_{2,new} &\equiv z_2, \quad z_{T,new} \equiv z_T \end{aligned} \quad (49)$$

$$\tau_{new} \equiv \tau = \tau(x) \quad (50)$$

Apparently, the properties of the updated and previous trajectories on the x-axis are identical, and the monotonicity of (41) remains.

The method of updating the trajectory is shown in Fig.10. The updated Bézier curve is determined by $L_{H,new}$, $P_{1,new}$, P_2 and T, which satisfies the constraint of zero miss distance and desired impact angle. According to the current position $M_H(x, z)$ and the heading angle ψ, interpolation points can be updated. Therefore, the additional equation to determine the new trajectory is formulated as

$$\begin{aligned} dz_{new}/dx_{new}\big|_{\tau_{new}} &= dz/dx\big|_{\tau} = -\tan\psi \\ z_{new}|_{\tau_{new}} &= z_{new}|_{\tau} = z \end{aligned} \quad (51)$$

Substituting (44) and (45) into (51) yields the following two equations.

$$\begin{aligned} &\frac{(1-\tau)^2 z_{L,new} - \left(3\tau^2 - 4\tau + 1\right) z_{1,new} + \left(3\tau^2 - 2\tau\right) z_2 - \tau^2 z_T}{(1-\tau)^2 x_L - \left(3\tau^2 - 4\tau + 1\right) x_1 + \left(3\tau^2 - 2\tau\right) x_2 - \tau^2 x_T} \\ &= -\tan\psi \\ &(1-\tau)^3 z_{L,new} + 3\tau(1-\tau)^2 z_{1,new} + 3\tau^2(1-\tau) z_2 + \tau^3 z_T \\ &= z \end{aligned} \quad (52)$$

The coordinates of the simulated initial states can be obtained as

$$\begin{bmatrix} z_{L,new} & z_{1,new} \end{bmatrix}^T = \boldsymbol{A}^{-1}\boldsymbol{B} \quad (53)$$

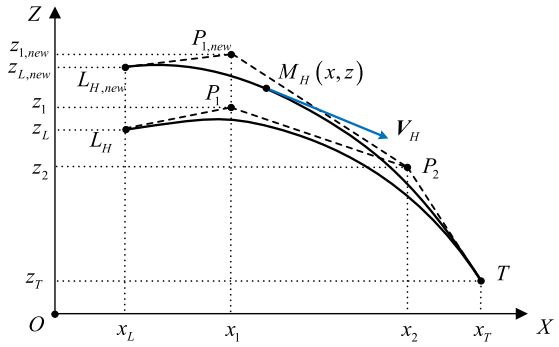

FIGURE 10. Updated and previous Bézier curve trajectories.

where the matrices $\boldsymbol{A}$ and $\boldsymbol{B}$ are defined as

$$\boldsymbol{A} = \begin{bmatrix} -3(1-\tau)^2 & 3\left(3\tau^2-4\tau+1\right) \\ (1-\tau)^3 & 3\tau(1-\tau)^2 \end{bmatrix}$$
$$\boldsymbol{B} = \begin{bmatrix} \tan(-\psi)\,dx/d\tau - 3\left(-3\tau^2+2\tau\right)z_2 - 3\tau^2 z_T \\ z - 3\tau^2(1-\tau)z_2 - \tau^3 z_T \end{bmatrix} \tag{54}$$

The inverse matrix $\boldsymbol{A}^{-1}$ is directly expressed as

$$\boldsymbol{A}^{-1} = \begin{bmatrix} -\tau/(\tau-1)^2 & (3\tau-1)/(\tau-1)^3 \\ -1/(3\tau-3) & 1/(\tau-1)^2 \end{bmatrix} (0 \le \tau < 1) \tag{55}$$

So there is always a unique solution to (53) before hitting the target. However, as τ approaches 1, (55) indicates that terminal singularity could exist. The update should terminate when τ is sufficiently close to 1, so that the accuracy will not be unduly affected. Because if the vehicle still deviates much when the update ceases, it can be determined that terminal constraints are not satisfied.

C. CONSTRAINED CONTROL COMMANDS

Normal acceleration a_{yn} and lateral acceleration a_{zn} are defined as

$$\begin{aligned} a_{yn} &= L\cos\sigma/m \\ a_{zn} &= L\sin\sigma/m \end{aligned} \tag{56}$$

Substitute (2) into (56) and rearrange it, lift coefficient can be expressed as

$$C_L = 2L/\left(\rho V^2 S_{ref}\right) = 2ma_{yn}/\left(\rho V^2 S_{ref}\cos\sigma\right) \tag{57}$$

Furthermore, the solution of the control is represented by a_{zn} and a_{yn} as

$$\begin{aligned} \sigma &= \arctan\left(a_{zn}/a_{yn}\right) \\ \alpha &= f_L^{-1}(M_a, C_L) = f_L^{-1}\left(M_a, 2ma_{yn}/\left(\rho V^2 S_{ref}\cos\sigma\right)\right) \end{aligned} \tag{58}$$

If the motion information can be measured and the projections in xy and xz plane can be solved, then a_m can be obtained in subsection A, and a_{zn} can be solved in subsection B. Hence

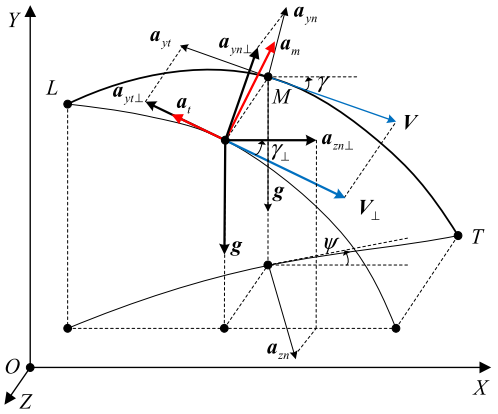

FIGURE 11. Decomposition of acceleration in three-dimensional environment.

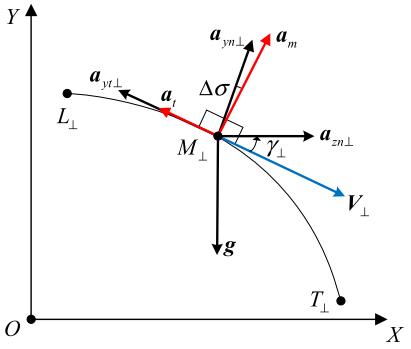

FIGURE 12. Decomposition of acceleration in xy plane.

the crux is to calculate the projection of each variable and determine the relationship between a_{yn}, a_{zn} and a_m.

The acceleration of the vehicle is decomposed in the flat earth model in Fig.11, where the real-time acceleration vector is the synthesis of vectors $\boldsymbol{a}_{yn}$, $\boldsymbol{a}_{yt}$, $\boldsymbol{a}_{zn}$ and $\boldsymbol{g}$. Fig.12 shows decomposition of acceleration in xy plane, where the vectors $\boldsymbol{a}_m$ and $\boldsymbol{a}_t$, synthesized by vectors $\boldsymbol{a}_{yn\perp}$, $\boldsymbol{a}_{yt\perp}$, $\boldsymbol{a}_{zn\perp}$ and $\boldsymbol{g}$, can be considered as total acceleration. Since vectors $\boldsymbol{V}$ and $\boldsymbol{a}_{yt}$ are collinear, their projections in xy plane are also collinear. In terms of the projections of the two vertical vectors $\boldsymbol{a}_{yn}$ and $\boldsymbol{a}_{yt}$ may intersect in xy plane, $\Delta\sigma$ depicts the angle between vectors $\boldsymbol{a}_{yn\perp}$ and $\boldsymbol{a}_m$.

When γ and ψ are given, the unit form of all vectors in Fig.11 can be expressed. Consequently, the projection vector of each unit vector on any plane and the corresponding projection angles can be solved. These angles are formulated as

$$\begin{aligned} \sigma_{a_{yn}} &= \arccos\left(\sqrt{1-\sin^2\psi\sin^2\gamma}\right) \\ \sigma_{a_{yt}} &= \arccos\left(\sqrt{1-\sin^2\psi\cos^2\gamma}\right) \\ \sigma_V &= \sigma_{a_{yt}} \end{aligned} \tag{59}$$

where the terms $\sigma_{a_{yn}}$, $\sigma_{a_{yt}}$ and σ_V are angles between vectors $\boldsymbol{a}_{yn}$, $\boldsymbol{a}_{yt}$, $\boldsymbol{V}$ and their projections $\boldsymbol{a}_{yn\perp}$, $\boldsymbol{a}_{yt\perp}$ and $\boldsymbol{V}_\perp$ in xy plane. Since the projection vectors and projection angles are

solved, several significant design parameters can be solved as (60)–(63), as shown at the bottom of this page.

Obviously, according to the rules of vector synthesis, the projection vector of normal acceleration in xy plane can be represented as

$$a_{yn\perp} = (a_m + g \cdot \cos(\gamma_\perp) + a_{zn} \cdot \sin\psi \cdot \sin\gamma_\perp) / \cos(\Delta\sigma) \tag{64}$$

Therefore, a_{yn} can be directly obtained from a_{zn} and a_m as

$$a_{yn} = \frac{a_{yn\perp}}{\cos(\sigma_{a_{yn}})} = \frac{a_m + g \cdot \cos(\gamma_\perp) + a_{zn} \cdot \sin\psi \cdot \sin\gamma_\perp}{\cos(\Delta\sigma) \cdot \cos(\sigma_{a_{yn}})} \tag{65}$$

From (65), motions in the two planes have been independently decoupled, and the normal acceleration command can be generated by compounding.

The final control command to be applied is ascertained by applying physical constraints and rate constraints. Therefore, a series of adjustments have been made to the desired control.

The effect of normal load constraint on acceleration command is formulated as follows:

$$\begin{cases} if\ \sqrt{a_{yn}^2 + a_{zn}^2} < n_{\perp\max} g, & \begin{cases} a_{yn}^1 = a_{yn} \\ a_{zn}^1 = a_{zn} \end{cases} \\ if\ \sqrt{a_{yn}^2 + a_{zn}^2} \geq n_{\perp\max} g, & \begin{cases} a_{yn}^1 = a_{yn} n_{\perp\max} g \Big/ \sqrt{a_{yn}^2 + a_{zn}^2} \\ a_{zn}^1 = a_{zn} n_{\perp\max} g \Big/ \sqrt{a_{yn}^2 + a_{zn}^2} \end{cases} \end{cases} \tag{66}$$

where the terms a_{yn}^1 and a_{yn}^1 are acceleration commands after preliminary adjustment. From (58), the initial control command can be obtained as

$$\begin{aligned} \sigma &= \arctan\left(a_{zn}^1 \Big/ a_{yn}^1\right) \\ \alpha &= f_L^{-1}\left(M_a, 2ma_{yn} \Big/ \left(\rho V^2 S_{ref} \cos\sigma\right)\right) \end{aligned} \tag{67}$$

Control adjustment caused by physical constraints is represented as

$$\begin{aligned} \sigma_1 &= \max(\min\sigma, \sigma_{\max}), \sigma_{\min}) \\ \alpha_1 &= \max(\min(\alpha, \alpha_{\max}), \alpha_{\min}) \end{aligned} \tag{68}$$

In terms of rate constraints, control command is finally modified as follows:

$$\begin{aligned} \sigma_2 &= \min\left(\sigma_{prev} + \left(t - t_{prev}\right)\dot{\sigma}_{\max}, \sigma_1\right) \\ \alpha_2 &= \min\left(\alpha_{prev} + \left(t - t_{prev}\right)\dot{\alpha}_{\max}, \alpha_1\right) \end{aligned}$$

$$\begin{aligned} \sigma_c &= \max\left(\sigma_{prev} - \left(t - t_{prev}\right)\dot{\sigma}_{\max}, \sigma_2\right) \\ \alpha_c &= \max\left(\alpha_{prev} - \left(t - t_{prev}\right)\dot{\alpha}_{\max}, \alpha_2\right) \end{aligned} \tag{69}$$

where the terms σ_2 and α_2 are intermediate control variables. The terms t_{prev}, α_{prev} and σ_{prev} are the time, angle of attack and bank angle magnitudes from previous calculation steps, respectively. The terms σ_c and α_c denote final control commands.

In conclusion, although the trajectory is designed with the idea of inverse dynamics, the acceleration command is derived from the decomposition method rather than directly from the desired trajectory shape in each plane. On the one hand, this method allows the trajectory in the two planes to be independently designed. On the other hand, acceleration commands are required, not the real-time trajectory shape which is unknown when applying a tracking method.

D. IMPLEMENTATION PROCESS OF GUIDANCE LAW

After the establishment of subsection A-C, the complete guidance process can be obtained as shown in Fig.13. In Fig.13, the term, e, represents the margin of error for Bézier guidance law. In this paper, the trajectory parameters (λ, k_1, k_2) are chosen fixed before the guidance procedure. In terms of constraints in (6) and (7), it seems difficult to predict the parameters of feasible nominal trajectories, mainly because the derivative of control is not directly related to the shape of trajectories. Consequently, trajectory parameters satisfying (16) and $0 < k_1 < k_2 < 1$ are all considered feasible. Simulation results in section IV show that a wide range of feasible trajectory parameters for the selected vehicle model are well acceptable.

IV. NUMERIC RESULTS AND DISCUSSION

To evaluate the performance and robustness of the proposed guidance law, several nominal cases and Monte Carlo simulations with dispersions and uncertainties are carried out. Due to the dispersion of aerodynamic coefficient and initial position, SMC method and real-time updating strategy are applied in vertical plane and lateral plane respectively.

A. NOMINAL TRAJECTORY DESIGN

It should be noted that, to implement the Bézier curve guidance law, the design conditions must be limited to $\gamma_T \in [-0.5\pi, 0)$ and $\psi_T \in (-0.5\pi, 0.5\pi)$. However, in the rotated xz coordinate system, the terminal heading angle can be adjusted to meet the design constraints.

$$V_H = V\cos\gamma \tag{60}$$

$$V_\perp = V\cos(\sigma_V) \tag{61}$$

$$\gamma_\perp = \arctan\left(\tan\gamma / \cos\psi\right) \tag{62}$$

$$\Delta\sigma = \arccos\left(\frac{\cos\psi}{\sqrt{\cos^2\psi\sin^2\gamma + \cos^2\gamma}\sqrt{\cos^2\psi\cos^2\gamma + \sin^2\gamma}}\right) \tag{63}$$

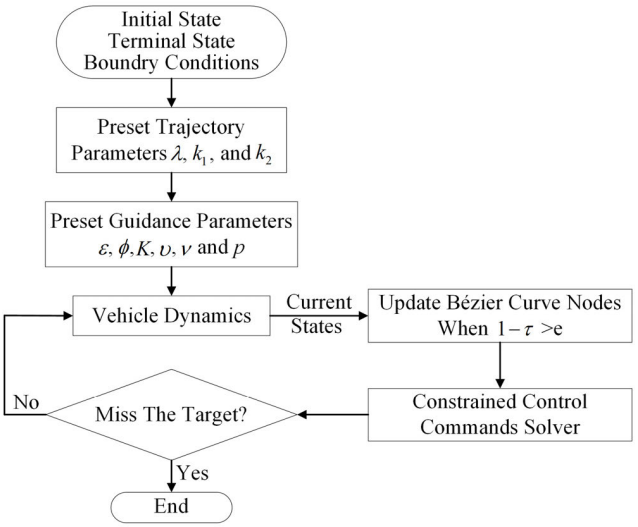

FIGURE 13. Guidance procedure.

TABLE 2. Desired trajectory properties for Fig. 14.

Cases	γ_L (deg)	γ_T (deg)	ψ_L (deg)	ψ_T (deg)
Case 1	20	-60	0	30
Case 2	20	-60	20	15
Case 3	20	-60	40	0
Case 4	40	-80	0	30
Case 5	40	-80	20	15
Case 6	40	-80	40	0

TABLE 3. Simulation boundary conditions.

Boundary conditions	x (km)	y (km)	z (km)	α (deg)	σ (deg)	V (m/s)
Initial conditions	0	30	-5	2	0	1800
End conditions	100	0	0			

To demonstrate the feasibility of geometric trajectory, the results of nominal trajectory design are given in this subsection. Table 2 shows desired trajectory properties, where launch point is located at (0 km, 30 km, −5 km), and target point is located at (100 km, 0 km, 0 km). Trajectory parameters are taken as $k_1 = 0.3$, $k_2 = 0.8$ and $\lambda = -10$ deg.

Various nominal elliptical trajectories in xy plane are depicted in Fig.14. It is worth noting that, as shown in the comparison of case 1, case 2 and case 3, elliptical trajectories vary with heading angles under fixed desired terminal flight path angles. This phenomenon occurs because xy plane is a projection plane fixed with reference frame, rather than the vertical plane containing the velocity vector.

Fig.15 shows the Bézier curve trajectories in xz plane. In contrast to Fig.14, there are three pairs of identical trajectories, because Bézier curves are determined only by the heading angles.

Fig.16 depicts the three-dimensional trajectories. The results show that the nominal trajectory can achieve the desired terminal flight path angle and heading angle, and can be further shaped by adjusting parameters k_1, k_2 and λ.

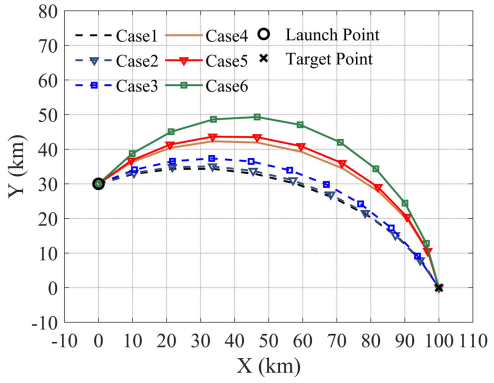

FIGURE 14. Nominal elliptical trajectories in xy plane.

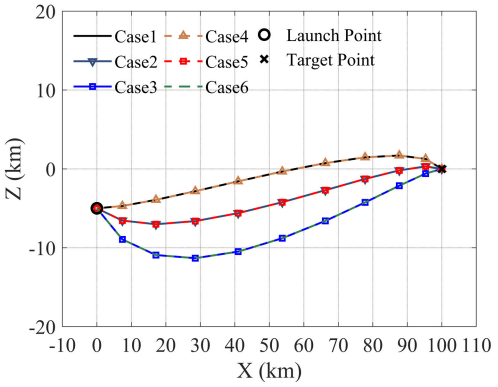

FIGURE 15. Nominal Bézier curve trajectories in xz plane.

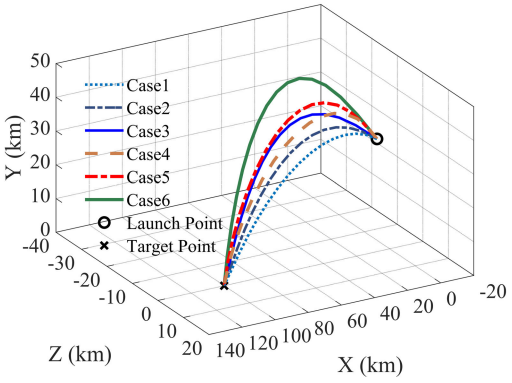

FIGURE 16. Three-dimensional geometric trajectories.

TABLE 4. Desired impact angles.

Case	γ_T (deg)	ψ_T (deg)
Case 1	-90	-35
Case 2	-90	15
Case 3	-70	-35
Case 4	-70	15
Case 5	-50	-35
Case 6	-50	15

B. NOMINAL CASES

endenumerate In this subsection, six nominal cases with various desired impact angles are adopted to verify the performance and applicability of the proposed method. The initial

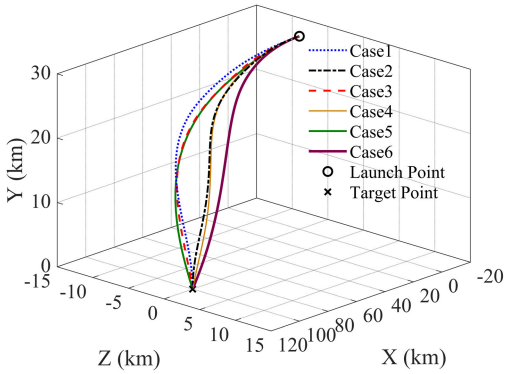

FIGURE 17. Three-dimensional trajectories.

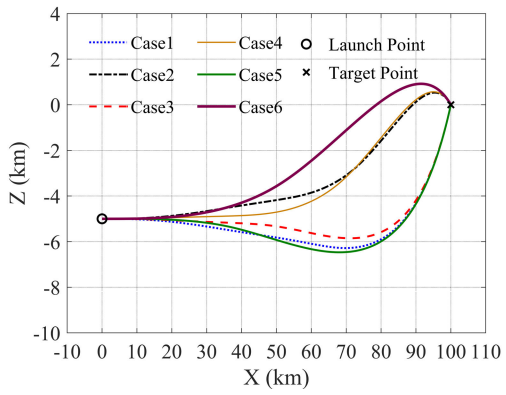

FIGURE 18. Real-time updated Bézier curve trajectories in *xz* plane.

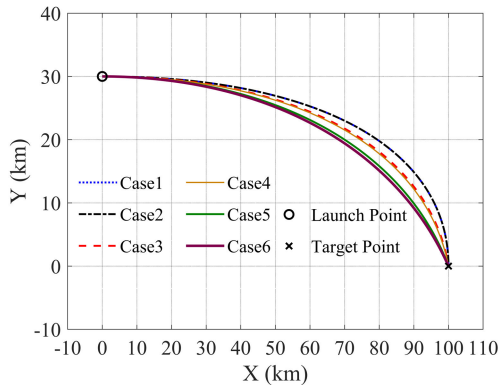

FIGURE 19. Trajectories in *xy* plane.

TABLE 5. Bounds of constraint limits.

Constraint limits	$n_\perp$ (m/s^2)	α (deg)	$\dot{\alpha}$ (deg/s)	σ (deg/s)	$\dot{\sigma}$ (deg/s)
Min value	0	-10	-3	-60	-10
Max value	20	10	3	60	10

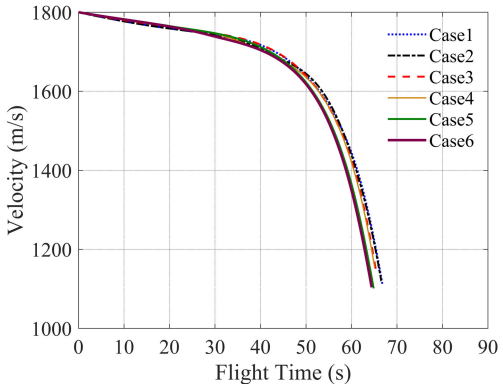

FIGURE 20. Velocity profiles.

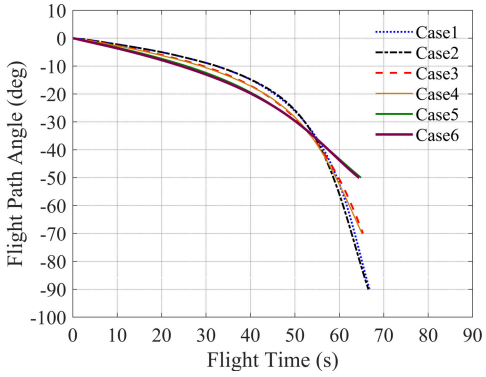

FIGURE 21. Flight path angle profiles.

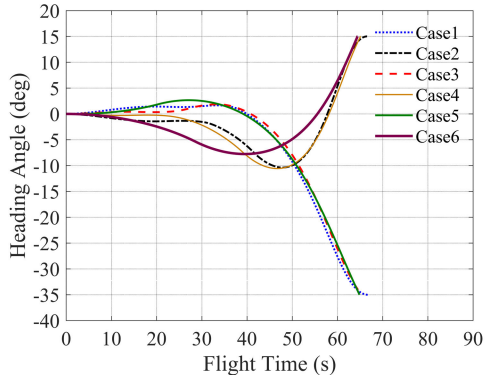

FIGURE 22. Heading angle profiles.

TABLE 6. Guidance and trajectory parameters.

Parameters	v	ν	p	ϕ	ε	K	k_1	k_2	λ (deg)
Value	100	0.3	8	30	70	0.04	0.3	0.8	10

and terminal boundary conditions for the simulated nominal cases are shown in Table 3. The desired terminal impact angles are listed in Table 4, and initial flight path angle and heading angle are 0 deg. Table 5 shows the upper and lower bounds of the constraints imposed on control commands. All trajectory design parameters and guidance parameters are listed in Table 6. Results of nominal simulations are shown in Fig.17-25.

The three-dimensional trajectories and their projections are depicted in Fig.17-19. Obviously, all trajectories start from the same origin and end at their destinations. Fig.20-22

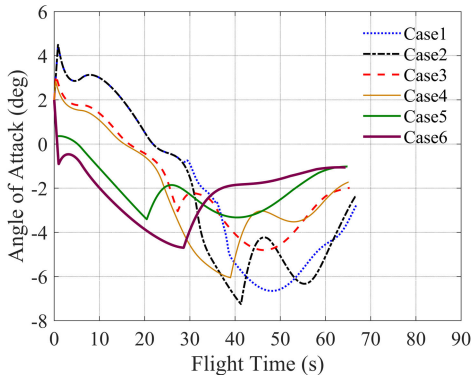

FIGURE 23. Angle of attack profiles.

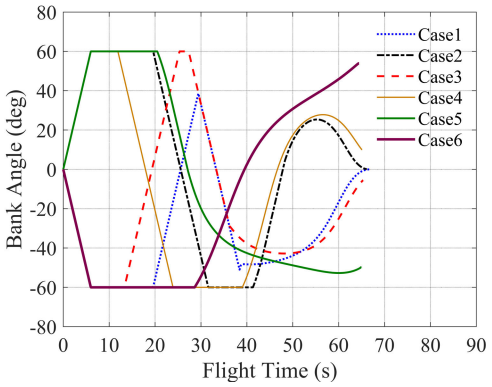

FIGURE 24. Bank angle profiles.

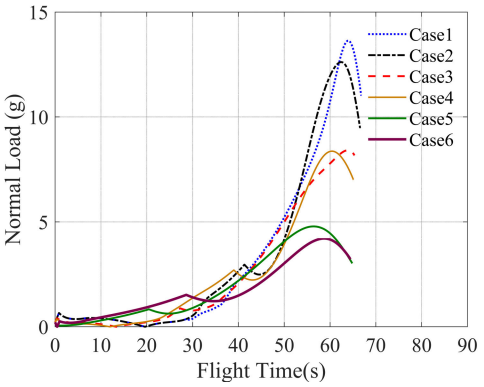

FIGURE 25. Normal load profiles.

shows the profiles of velocity, flight path angle and heading angle, respectively. Although the terminal velocity is not controlled, its dispersion range is not wide, while the flight path angle and heading angle both reach the specified terminal value accurately. Fig.23 illustrates angle of attack profiles, which continuously change without reaching the boundary. The terminal radius of curvature obviously affects the rate of terminal angle of attack, therefore it is necessary to choose an appropriate λ. To be a contrast, as shown in Fig.24, bank angle maintains its boundary value for a long

TABLE 7. Final state errors for various cases.

Case	Miss distance (m)	Flight path angle error (deg)	Heading angle error (deg)
Case1	3.1811×10^{-3}	2.6982×10^{-5}	-7.9832×10^{-3}
Case2	3.8945×10^{-3}	4.3416×10^{-8}	1.1406×10^{-2}
Case3	1.0817×10^{-3}	1.7846×10^{-4}	7.3038×10^{-4}
Case4	4.8844×10^{-4}	6.9882×10^{-5}	6.4378×10^{-4}
Case5	1.3366×10^{-4}	-3.2004×10^{-5}	7.8017×10^{-5}
Case6	2.0218×10^{-3}	-9.6036×10^{-6}	-1.0184×10^{-4}

TABLE 8. Statistics of dispersion in 500 Monte Carlo runs.

Dispersion	Parameter	Distribution	3σ/Range
Initial condition	x	Normal	±1500m
	y	Normal	±1500m
	z	Normal	±1500m
	V	Normal	±150m/s
	γ	Normal	±1deg
	ψ	Normal	±1deg
Aerodynamic modeling	C_L	Normal	±15%
	C_D	Normal	±15%
Atmospheric modeling	ρ	Normal	±10%

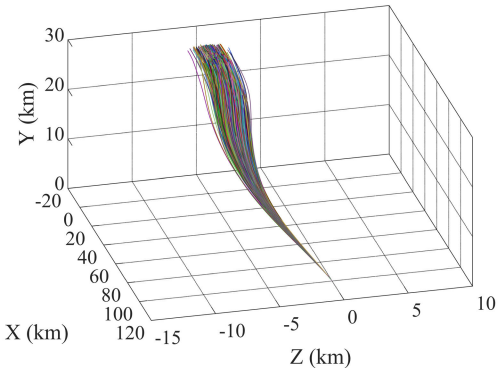

FIGURE 26. Three-dimensional trajectories.

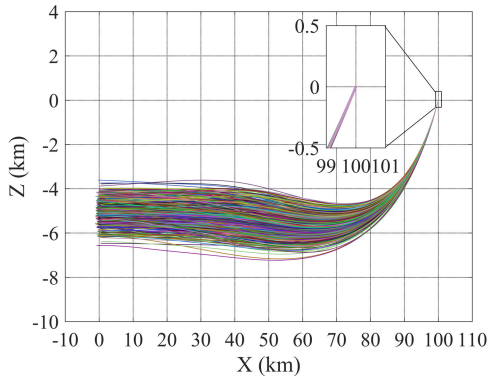

FIGURE 27. Trajectories in *xz* plane.

time due to insufficient lateral maneuver-ability. Therefore, the real-time update strategy in lateral plane is essential and effective. Fig.25 depicts the profiles of load during the flights. Obviously, all path constraints are enforced strictly.

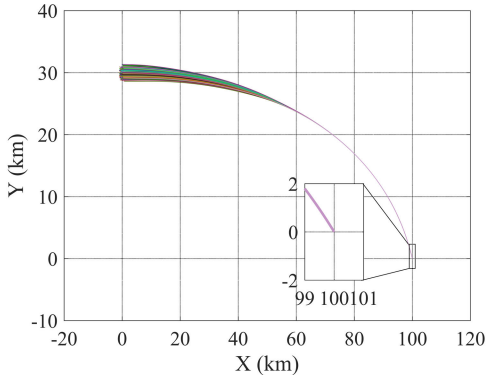

FIGURE 28. Trajectories in *xy* plane.

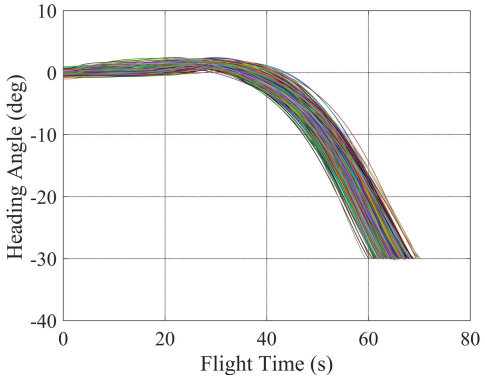

FIGURE 31. Heading angle profiles.

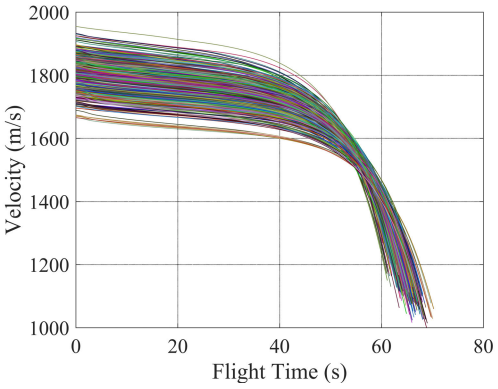

FIGURE 29. Velocity profiles.

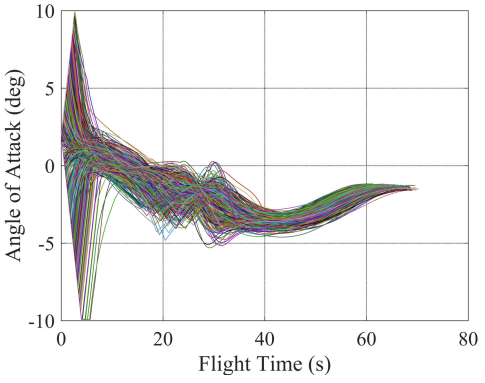

FIGURE 32. Angle of attack profiles.

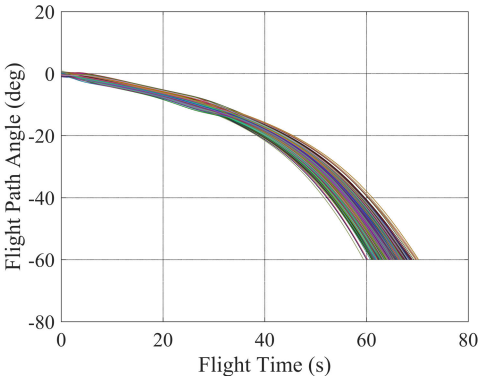

FIGURE 30. Flight path angle profile.

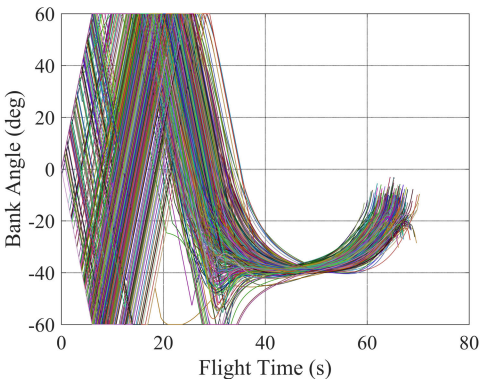

FIGURE 33. Bank angle profiles.

Table 7 summarizes the statistics of final state errors for various cases. All miss distances are not greater than 0.01m, and all flight path angle and heading angle errors are not greater than 0.02deg. Due to stop criterion of real-time update, the error of heading angle is slightly larger than the error of flight path angle. The nonlinear system tracking ellipse is stable, and the real-time updating of Bézier curve is convergent. In general, the simulation results of nominal cases show that the proposed guidance law is effective.

C. MONTE CARLO SIMULATIONS

In this subsection, to further evaluate the performance and robustness of the proposed guidance law, 500-run Monte Carlo simulations are conducted under a wide distribution of random dispersions and uncertainties which are listed in Table 8.

The dispersions and uncertainties in Table 8 include not only aerodynamic coefficients and atmospheric density, which strongly affect the dynamics, but also initial conditions. Initial and terminal boundary conditions are listed in Table 3. Results of 500-run Monte Carlo simulations are depicted in Fig.26-34.

As shown in Fig.26, despite the dispersion and uncertainties, the vehicle hits the target accurately. Fig.27 displays Bézier trajectories in *xz* plane, which are scattered in the early stage to fit bank angle constraint, and finally converges

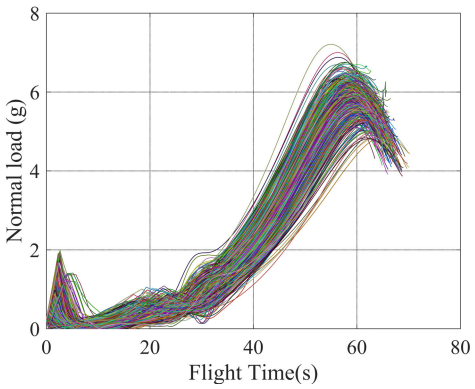

FIGURE 34. Normal load profiles.

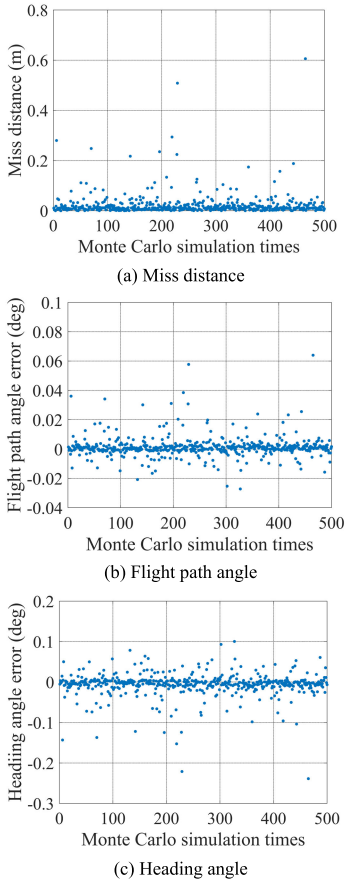

FIGURE 35. Statistics of terminal errors for the 500 runs.

steadily to the target. Trajectories in *xy* plane are depicted in Fig.28. Obviously, the vehicle approaches the nominal ellipse in *xy* plane quickly and smoothly, and then follows closely. The proposed ISMC guidance method corrects the deviation in the early stage and meets the severe terminal strike requirements at the same time. Fig.29 shows velocity profiles. The terminal velocity distribution for the 500-run Monte Carlo simulations is almost within 200 m/s. Profiles of flight path angle and heading angle are shown in Fig.30 and Fig.31, respectively. It is apparent that desired impact angle is achieved under perturbation. Fig.32 depicts angle of attack profiles. Although the early trajectory adjustment may require its maximum, the angle of attack changes steadily near terminal moment. By contrast, as shown in Fig.33, bank angle changes relatively drastically, and its threshold is taken for a long time. The terminal rate of bank angle is relatively obvious and the sign is uncertain. Fig.34 displays profiles of normal load, which is always below its limit.

Statistics of terminal errors for the 500 runs are shown in Fig.35. All miss distances are mostly within 0.1 m and the maximum is within 0.8 m. All angular errors are within 0.2 deg. The results show that the proposed method is robust and has strong engineering practicability for the hypersonic model selected in this paper.

V. CONCLUSION

In this paper, a novel three-dimensional geometric guidance law with terminal impact angle constraint is proposed, which is implemented by controlling the launch point, aircraft, and target on a certain curve. The nominal trajectory in the vertical plane is an adjustable elliptic curve that satisfies terminal angle constraint, and elliptic equations for different rotation angles of main axis are given. The ISMC method is employed to track the nominal elliptical trajectory, which effectively reduces the trajectory vibration. The online planning strategy of updating the third-order Bézier curve is adopted in lateral plane due to inadequate lateral maneuverability. The nominal trajectories in two planes can be greatly shaped by adjusting the trajectory parameters. To verify the effectiveness of the proposed guidance law, 500-run simulations are carried out considering perturbations in the initial state, and error in aerodynamic and atmospheric modelling. The experimental results indicate that the proposed guidance law has strong adjustability and excellent robustness.

In this paper, both the ISMC tracking method and the real-time update strategy are employed in the lateral plane. The significant geometric difference between the two methods is that the radius of curvature is controllable for tracked trajectories, while for real-time updated trajectories is unpredictable due to control constraints. Since there is a gravitational acceleration in the vertical plane, the sign of the resultant normal acceleration is related to radius of curvature. Obviously, if the tracking method is utilized in two planes simultaneously, it is difficult to meet the control constraints. When simultaneous updating strategy is adopted, the bank angle is prone to be reversed frequently in case of demanding lateral maneuvers (like case 2, 4 and 6 in Table 4), which could result in missing the target.

The acceleration commands in the two fixed planes are decoupled by decomposition method, so the guidance law is independent of range-to-go. At the same time, it renders it possible to combine various analytic curves in two planes. In the future, more complex constraints and optimality may be realized by adjusting trajectory parameters or selecting more efficient analytic curves.

REFERENCES

[1] B. S. Kim, J. G. Lee, and H. S. Han, "Biased PNG law for impact with angular constraint," *IEEE Trans. Aerosp. Electron. Syst.*, vol. 34, no. 1, pp. 277–288, 1998.

[2] K. S. Erer and O. Merttopçuoglu, "Indirect impact-angle-control against stationary targets using biased pure proportional navigation," *J. Guid., Control, Dyn.*, vol. 35, no. 2, pp. 700–704, Mar. 2012.

[3] T.-H. Kim, B.-G. Park, and M.-J. Tahk, "Bias-shaping method for biased proportional navigation with terminal-angle constraint," *J. Guid., Control, Dyn.*, vol. 36, no. 6, pp. 1810–1816, Nov. 2013.

[4] B.-G. Park, T.-H. Kim, and M.-J. Tahk, "Biased PNG with terminal-angle constraint for intercepting nonmaneuvering targets under physical constraints," *IEEE Trans. Aerosp. Electron. Syst.*, vol. 53, no. 3, pp. 1562–1572, Jun. 2017.

[5] A. Ratnoo and D. Ghose, "Impact angle constrained interception of stationary targets," *J. Guid., Control, Dyn.*, vol. 31, no. 6, pp. 1817–1822, Nov. 2008.

[6] R. Tekin and K. S. Erer, "Switched-gain guidance for impact angle control under physical constraints," *J. Guid., Control, Dyn.*, vol. 38, no. 2, pp. 205–216, Feb. 2015.

[7] B.-G. Park, H.-H. Kwon, Y.-H. Kim, and T.-H. Kim, "Composite guidance scheme for impact angle control against a nonmaneuvering moving target," *J. Guid., Control, Dyn.*, vol. 39, no. 5, pp. 1132–1139, May 2016.

[8] X. Liu, Z. Shen, and P. Lu, "Closed-loop optimization of guidance gain for constrained impact," *J. Guid., Control, Dyn.*, vol. 40, no. 2, pp. 453–460, Feb. 2017.

[9] M. Kim and K. Grider, "Terminal guidance for impact attitude angle constrained flight trajectories," *IEEE Trans. Aerosp. Electron. Syst.*, vol. AES-9, no. 6, pp. 852–859, Nov. 1973.

[10] C.-K. Ryoo, H. Cho, and M.-J. Tahk, "Optimal guidance laws with terminal impact angle constraint," *J. Guid., Control, Dyn.*, vol. 28, no. 4, pp. 724–732, Jul. 2005.

[11] V. Shaferman and T. Shima, "Linear quadratic guidance laws for imposing a terminal intercept angle," *J. Guid., Control, Dyn.*, vol. 31, no. 5, pp. 1400–1412, Sep. 2008.

[12] A. Ratnoo and D. Ghose, "SDRE based guidance law for impact angle constrained trajectories," in *Proc. AIAA Guid., Navigat. Control Conf. Exhibit*, vol. 3, Aug. 2007, pp. 2202–2217.

[13] A. Ratnoo and D. Ghose, "State-dependent Riccati-equation-based guidance law for impact-angle-constrained trajectories," *J. Guid., Control, Dyn.*, vol. 32, no. 1, pp. 320–326, Jan. 2009.

[14] I. Taub and T. Shima, "Intercept angle missile guidance under time varying acceleration bounds," *J. Guid., Control, Dyn.*, vol. 36, no. 3, pp. 686–699, May 2013.

[15] B.-G. Park, T.-H. Kim, and M.-J. Tahk, "Optimal impact angle control guidance law considering the seeker's field-of-view limits," *Proc. Inst. Mech. Eng. G, J. Aerosp. Eng.*, vol. 227, no. 8, pp. 1347–1364, Jun. 2012.

[16] B.-G. Park, T.-H. Kim, and M.-J. Tahk, "Range-to-go weighted optimal guidance with impact angle constraint and seeker's look angle limits," *IEEE Trans. Aerosp. Electron. Syst.*, vol. 52, no. 3, pp. 1241–1256, Jun. 2016.

[17] J. Zhu, D. Su, Y. Xie, and H. Sun, "Impact time and angle control guidance independent of time-to-go prediction," *Aerosp. Sci. Technol.*, vol. 86, pp. 818–825, Mar. 2019.

[18] S. R. Kumar, S. Rao, and D. Ghose, "Nonsingular terminal sliding mode guidance with impact angle constraints," *J. Guid., Control, Dyn.*, vol. 37, no. 4, pp. 1114–1130, Jul. 2014.

[19] X. Wang, Y. Zhang, and H. Wu, "Sliding mode control based impact angle control guidance considering the seeker's field-of-view constraint," *ISA Trans.*, vol. 61, pp. 49–59, Mar. 2016.

[20] Z. Hou, Y. Yang, L. Liu, and Y. Wang, "Terminal sliding mode control based impact time and angle constrained guidance," *Aerosp. Sci. Technol.*, vol. 93, Oct. 2019, Art. no. 105142.

[21] S. Xiong, W. Wang, X. Liu, S. Wang, and Z. Chen, "Guidance law against maneuvering targets with intercept angle constraint," *ISA Trans.*, vol. 53, no. 4, pp. 1332–1342, Jul. 2014.

[22] Z. Zhang, S. Li, and S. Luo, "Terminal guidance laws of missile based on ISMC and NDOB with impact angle constraint," *Aerosp. Sci. Technol.*, vol. 31, no. 1, pp. 30–41, Dec. 2013.

[23] Y. Ji, D. Lin, W. Wang, S. Hu, and P. Pei, "Three-dimensional terminal angle constrained robust guidance law with autopilot lag consideration," *Aerosp. Sci. Technol.*, vol. 86, pp. 160–176, Mar. 2019.

[24] R. Tekin and F. Holzapfel, "Impact angle control based on feedback linearization," in *Proc. AIAA Guid., Navigat., Control Conf.*, Jan. 2017, doi: 10.2514/6.2017-1509.

[25] B. Liu, M. Hou, and D. Feng, "Nonlinear mapping based impact angle control guidance with seeker's field-of-view constraint," *Aerosp. Sci. Technol.*, vol. 86, pp. 724–736, Mar. 2019.

[26] T.-H. Kim, C.-H. Lee, and M.-J. Tahk, "Time-to-go polynomial guidance laws with terminal impact angle/acceleration constraints," *IFAC Proc. Volumes*, vol. 44, no. 1, pp. 3915–3919, Jan. 2011.

[27] T.-H. Kim, C.-H. Lee, I.-S. Jeon, and M.-J. Tahk, "Augmented polynomial guidance with impact time and angle constraints," *IEEE Trans. Aerosp. Electron. Syst.*, vol. 49, no. 4, pp. 2806–2817, Oct. 2013.

[28] O. A. Yakimenko, "Direct method for rapid prototyping of near-optimal aircraft trajectories," *J. Guid., Control, Dyn.*, vol. 23, no. 5, pp. 865–875, Sep. 2000.

[29] J. A. Lukacs and O. A. Yakimenko, "Trajectory-shaping guidance for interception of ballistic missiles during the boost phase," *J. Guid., Control, Dyn.*, vol. 31, no. 5, pp. 1524–1531, Sep. 2008.

[30] A. Naghash, R. Esmaelzadeh, M. Mortazavi, and R. Jamilnia, "Near optimal guidance law for descent to a point using inverse problem approach," *Aerosp. Sci. Technol.*, vol. 12, no. 3, pp. 241–247, Apr. 2008.

[31] H. Zhou, T. Rahman, and W. Chen, "Neural network assisted inverse dynamic guidance for terminally constrained entry flight," *Sci. World J.*, vol. 2014, Feb. 2014, Art. no. 686040.

[32] H. Zhou, T. Rahman, and W. Chen, "Impact angle and impact velocity constrained terminal guidance for stationary target," *Aircr. Eng. Aerosp. Technol.*, vol. 87, no. 5, pp. 454–464, Sep. 2015.

[33] I. R. Manchester and A. V. Savkin, "Circular navigation guidance law for precision missile/target engagements," in *Proc. 41st IEEE Conf. Decis. Control*, vol. 2, 2002, pp. 1287–1292.

[34] M.-G. Yoon, "Relative circular navigation guidance for the impact angle control problem," *IEEE Trans. Aerosp. Electron. Syst.*, vol. 44, no. 4, pp. 1449–1463, Oct. 2008.

[35] R. Tsalik and T. Y. Shima, "Inscribed angle guidance," in *Proc. AIAA Guid., Navigat., Control (GNC) Conf.*, 2013, doi: 10.2514/6.2013-4952.

[36] R. Tsalik and T. Shima, "Inscribed-angle guidance against moving targets," *J. Guid., Control, Dyn.*, vol. 40, no. 12, pp. 3211–3225, Dec. 2017.

[37] T. Zhang and H. She, "Elliptical trajectory guidance law with terminal impact angle constraint," in *Proc. AIAA Atmos. Flight Mech. Conf.*, Jan. 2015, 10.2514/6.2015-1021.

[38] R. Livermore, R. Tsalik, and T. Shima, "Elliptic guidance," *J. Guid., Control, Dyn.*, vol. 41, no. 11, pp. 2435–2444, Nov. 2018.

[39] C. Anderson, *Curves and Surfaces in Computer Aided Geometric Design*, vol. 32, no. 2. Technometrics, 1990, doi: 10.1080/00401706.1990.10484650.

HAO ZHOU was born in 1976. He received the B.S. degree in aerodynamics from the National University of Defense Technology, Changsha, China, in 1998, and the Ph.D. degree in aerospace engineering from Beihang University, Beijing, China, in 2006. Since 2006, he has been a Lecturer with the School of Astronautics, Beihang University. His research interests include flight dynamics, guidance and control, and trajectory optimization.

TAO CHENG was born in 1996. He received the B.S. degree in flight vehicle design from Beihang University, Beijing, China, in 2018, where he is currently pursuing the master's degree. His research interests include flight dynamics, and guidance and control.

XIAOMING LIU was born in Shandong, China, in 1982. He received the Ph.D. degree in aerospace engineering from Beihang University, Beijing, China, in 2011. Since 2013, he has been a Lecturer with the School of Astronautics, Beihang University. His research interests include flight mechanics, navigation guidance and control, information fusion, and sensors applications.

WANCHUN CHEN was born in 1964. He received the B.S. and M.S. degrees in flight vehicle design from Beihang University, in 1986 and 1989, respectively, and the Ph.D. degree in flight dynamics and control from BUAA, in 1995. Since 1991, he has been with the School of Astronautics, BUAA, where he is currently a Professor. His research interests include flight dynamics and control of aerospace vehicle, and aerospace vehicle integrated design and analysis.